Optical and Quantum Electronics (2024) 56:374
https://doi.org/10.1007/s11082-023-05909-z

Removal of Atrazine from contaminated water by functionalized graphene quantum dots

Ahmed Hellal[1] · Hazem Abdelsalam[2] · Walid Tawfik[1] · Medhat A. Ibrahim[3,4]

Received: 16 October 2023 / Accepted: 21 November 2023 / Published online: 2 January 2024

Abstract
The limitation of clean water supplies and the increment of water pollution resources, like industrial processes, oil pollution, and herbicides, are urgent reasons for introducing new techniques for treating contaminated water. Atrazine is heavily used as a herbicide due to its high effectiveness and low price. However, its environmental persistence causes water contamination, and human exposure to Atrazine is linked to several health effects. This work presents a simulation study of the possibility of removing the Atrazine from water by functionally activated graphene quantum dots (GQDs), using density functional theory (DFT) at B3LYP/3-21G level. The activity of GQDs C46 with a total dipole moment of 0.9 is enhanced by the attachment of chemical groups; for instance, attaching CN and NO_2 groups increases the total dipole moment to 8.744 and 9.123, respectively. The effect of the functionalized groups Carboxyl and cyanide was investigated, and confirmed that there was no structure deformation due to the functionalization process. Analysis of the obtained data shows the remarkable adsorption ability of GQDs activated by CN and NO_2 groups toward the removal of atrazine herbicides due to positive adsorption energy 1.31, 128, and 1.3 eV obtained from pristine, carboxyl graphene, and cyanide graphene respectively. According to the calculated total charge on the complexes Atrazine and GQDs and Functionalized GQD, charge transfer mainly depends on the interaction pattern. The values of charges were − 0.02, 0.004, and − 0.004 for pristine, carboxyl, and cyanide graphene, respectively. Therefore, the observed results demonstrated the possibility of applying the chemically modified carbon quantum dots as a potential candidate for the treatment of contaminated water.

Keywords Wastewater · Graphene quantum dots · ZTRI · DFT and Atrazine

✉ Medhat A. Ibrahim
medahmed6@yahoo.com

[1] Department of Laser in Meteorology, Photochemistry and Agriculture (LAMPA), National Institute of Laser Enhanced Sciences, Cairo University, Giza 12266, Egypt

[2] Department of Theoretical Physics, National Research Centre, Giza 12622, Egypt

[3] Spectroscopy Department, National Research Centre, Giza 12622, Egypt

[4] Molecular Modeling and Spectroscopy Laboratory, Centre of Excellence for Advanced Science, National Research Centre, 33 El-Bohouth St., Dokki, Giza 12622, Egypt

1 Introduction

Pesticide is a descriptive word for many chemicals used in the agriculture sector. It can be classified as but not limited to insecticides, herbicides, fungicides, rodenticides, nematicides, etc. Pesticides play an essential role in increasing world crop production. Nearly 45% of crop production is lost because of pest invasion, and this percentage tends to increase in tropical areas due to suitable conditions for pest enhancement multiplications (Abhilash and Singh 2009). Atrazine is a chlorotriazine herbicide. It consists of a ring structure called the triazine ring, five nitrogen atoms, and a chlorine atom (2-chloro-4-methylamino-6-isopropylamino-1,3,5-riazine). Atrazine is a member of an s-thiazine group of herbicides introduced in the market as an agrochemical since the 1970s; it continues to be applied to crops in the U.S., China, Australia, and elsewhere even though it has been banned in the European Union. Since that time, it has been considered one of the publicly used herbicides because of its effectiveness to remove a wide range of undesirable weeds and algae with an average use 70,000–90,000 tons applied per year (Das et al. 2023; Christian et al. 1995; Sass and Colangelo 2006). Atrazine is almost non-volatile, and its half-life in neutral conditions is about 200 days, but varies from 4 to 57 weeks depending on various environmental factors such as pH, moisture content, temperature, and microbial activity (Burnside and Wicks 1980; Carsel et al. 1985; McCormick and Hiltbold 1966). As a result of their structural properties and water solubility, atrazine pesticides have persistent occurrence and are detectable in surface water bodies, causing degradation in their quality (Michael et al. 1992; Mariane et al. 2020). Fish and other aquatic animals consume such contaminated water, which bio-accumulates in their bodies, giving other reasons to increase these environmental pollutants through the food chain (Karr and Chu 2000). This herbicide can cause an endocrine disruptor genic effect and epidemiological connection to low sperm levels in men; therefore, it was recommended that atrazine be banned in the U.S. Exposure to atrazine can be harmful and, in extreme cases, can cause health problems (Allran and Karasov 2009). Therefore, it is most important to develop reliable and effective techniques for the removal of atrazine from natural environments (Das et al. 2023).

One of the most beneficial approaches to remove contaminants from the environment is to employ nanotechnology to face such environmental challenges (Xiaolei et al. 2013). Over the past few decades, graphene and graphene-based compounds have captured the attention of many researchers. Graphene is composed of a two-dimensional layer of carbon atoms closely packed in a honeycomb shape, and can be used to create numerous new classes of sorbent materials that are efficient at adsorbing contaminants from polluted water (Xiaolei et al. 2013; Xu et al. 2012; Zhang et al. 2013a; Yang et al. 2010; Fan et al. 2022). The importance of this class of compounds comes from possessing some electronic properties including thermal mobility, mechanical strength, and tunable band gap energy that enable them to be utilized in many applications (Zhang et al. 2013b; Geim and Novoselov 2007; Owen et al. 2010). Additionally, graphene-based materials are characterized by their low cost and high surface area, theoretically estimated at 2630 $m^2\ g^{-1}$. These outstanding properties promote graphene as a unique option for the adsorption of environmental contaminants. The chemical and electronic properties of Graphene can even be further enhanced by functionalization. For instance, Hazem et al. (2018) demonstrated that the functionalization of graphene with a carboxyl group (–COOH) significantly increased the total dipole moment (TDM) to 4.033 (D), which reflects strong reactivity toward the surrounding medium (Abdelsalam et al. 2018).

In this paper, using density functional theory (DFT) calculations we investigated different scenarios for the adsorption of atrazine on graphene quantum dots functionalized by many groups, including carboxylic, cyanide, and nitrogen oxide groups. Many active sites were suggested for the adsorption to take place through.

2 Calculation details

The unparalleled success of density functional theory (DFT) in explaining materials phenomena has led to the concept of 'materials by design the idea that for any given set of properties, we can predict novel materials that outperform any known 'usual suspects. (Hasnip et al. 2014). In this study, we use a powerful calculation tool of DFT (Hohenberg and Kohn 1964; Kohn and Sham 1965) to estimate the most proper sites on ZTRI Graphene functionalized by different activation groups to adsorb Atrazine. The DFT is implemented in Gaussian 09 (Frisch et al. 2009), which utilizes a basis set of Gaussian-type orbital functions. The Becke-style three-parameters-Lee–Yang–Parr hybrid functional B3LYP with split-valence basis sets of this type: 3-21G (Axel 1993) for Atrazine and adsorption process state (Rudberg et al. 2007) both are implemented in personal computer at Molecular Modeling and Spectroscopy Laboratory, Centre of Excellence for Advanced Science, National Research Centre. Different ways were studied for the adsorption of Atrazine on functionalized graphene quantum dots: (a) adsorption on the edges of the pristine ZTRI (b) adsorption on the edges of the ZTRI functionalized by carboxylic group, and (c) adsorption on the edges of the ZTRI functionalized by cyanide group interacting with functionalized. The adsorption energy, charge transfer, and band gap energy are calculated to demonstrate the effect of different functionalization groups in the atrazine adsorption process.

3 Results and discussion

3.1 Stability of optimized structures

Triangular graphene quantum dots (ZTRI) are optimized using B3LYP/3-21G level of calculation without symmetry constraint using Gaussian 09. The optimization showed little increase of about 1.5% overall in the C-H bond in ZTRI to be 1.086 Å compared to 1.07 Å bond length before optimization. All C–C bonds adjusted after optimization to be in the range of 1.39–1.45 Å compared to 1.4 Å in the unoptimized one. The bond angle between (C–C–C) was 120° fixed overall unoptimized structure, but it is slightly changed in the optimized structure to range from 118.6° to 122.0° where the most open angles were in the edge outside, as demonstrated in Fig. 1.

ZTRI has been studied by adding different functionalized groups. The capability of ZTRI to adsorb atrazine is estimated by activation either using a carboxylic group or cyanide group on one edge of the triangle of ZTRI. The optimized structure of carboxylate Graphene and cyno–graphene compared to ZTRI, in C–C bond length dcc, C-H bond length $d_{CH,}$ and C–C–C bond angles shown in Fig. 2 and Table 1.

Figure 2 indicates that there is no significant change in graphene structure by adding any functionalizing groups, and the geometric shape of ZTRI is not deformed. The optimized structure demonstrated in Fig. 3 of Atrazine at B3LYP/3-21G showed total energy was – 1041.84 Hartree's, whereas band gap energy which was calculated as a

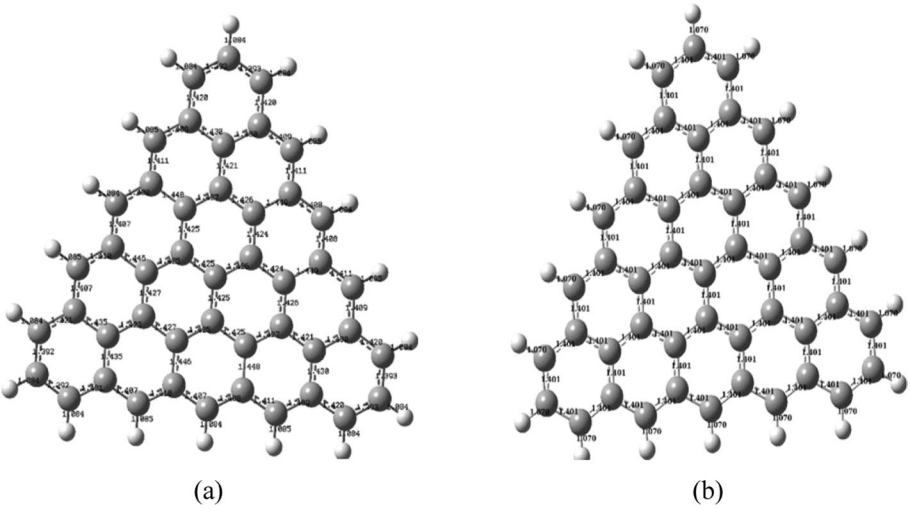

Fig. 1 Graphene quantum dots (ZTRI) C–C and C–H bond length **a** before and **b** after optimization

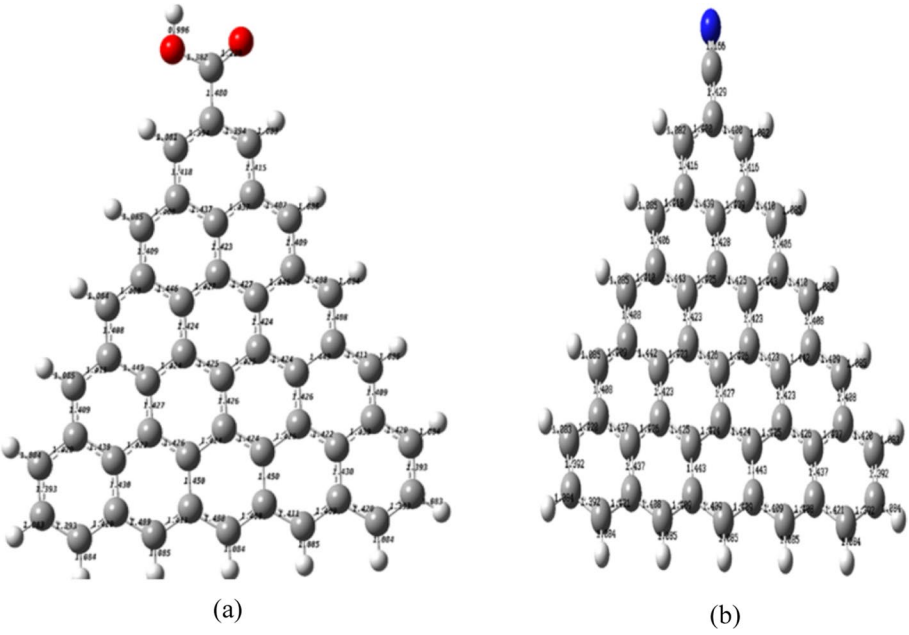

Fig. 2 Bond length in **a** ZTRI-COOH and **b** ZTRI-CN after optimization

difference between HOMO–LUMO was 5.99 eV this outcome validated and agree with Atrazine optimized outcomes data from Luis Humberto et al. (2010) (Huizar et al. 2015) using B3LYP/6–311++G (2d, 2p) level which recorded − 1047.50 Hartree and 5.91 eV respectively.

Table 1 The C–H and C–C bond lengths, and C–C–C bond angles

Structure	d_{C-H} (Å)	d_{C-C} (Å)	C–C–C (°C)
ZTRI pristine	1.07	1.4	119.99–120
ZTRI optimized	1.084	1.39–1.45	118.6–122
ZTRI-COOH	1.081–1.085	1.39–1.44	118.7–122.5
ZTRI-CN	1.083–1.085	1.39–1.43	118.5–122.5

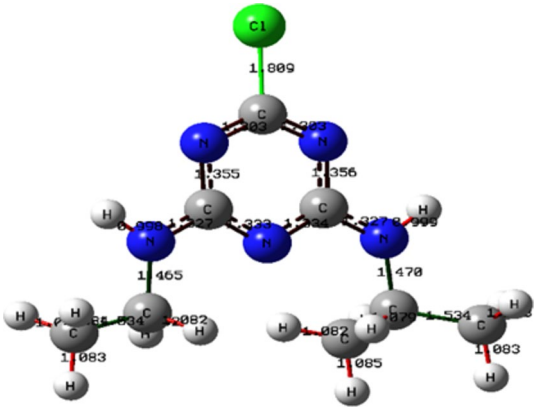

Fig. 3 Atrazine optimized structure

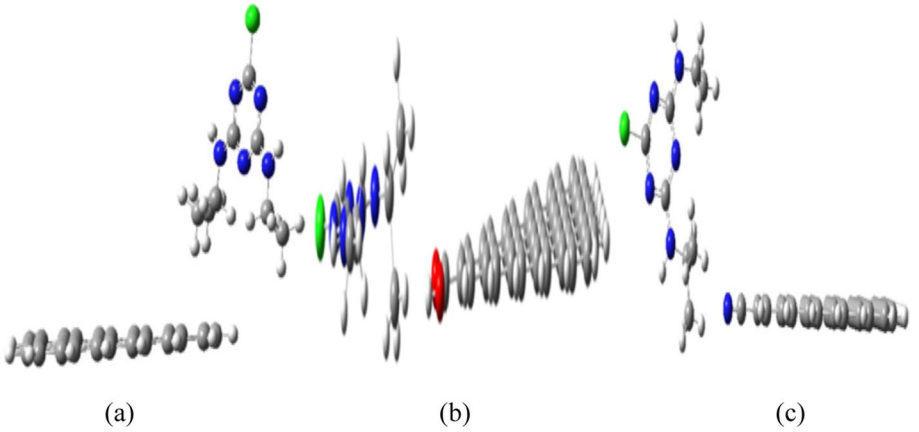

Fig. 4 Adsorption mechanism of atrazine on **a** pristine graphene edge **b** carboxylate graphene and **c** cyanide graphene

The mechanism used to estimate the interaction between ZTRI and different functionalized ZTRI with Atrazine is by approaching Terminal H (H17) atom from three carbon side of Atrazine to (Edge H atom of un-functionalized ZTRI, H atom of the hydroxyl group of carboxylate Z.T.R. and finally Nitrogen atom of cyanide group in ZTR C46 functionalized by cyanide group) Edge-to-edge with distance 1.8, 2.27 and 2.49 Å respectively, to show the effect of different functionalized group in the adsorption process as shown in Fig. 4.

3.2 Chemical reactivity and adsorption process

The TDM of ZTRI has a non-zero value of approx. 0.9 Debye. This is a result of the slight electronegativity difference between carbon and hydrogen atoms. 0.35 Pauling (Ouellette and Rawn 2014) in outer frame combined with the effect of geometrical shape because an odd number of sides three heads in ZTRI triangles shape which can't cancel each other causing constant slight partial polarity (Abdelsalam et al. 2018) dipole moments provide information about a molecule's polarity, anisotropy, and reactivity in addition to its polarity (Hiroaki et al. 2011). A dramatic increase in TDM has been observed in functionalized ZTRI by adding either a carboxylic or cyanide group on the head side. The TDM was calculated to be 2.75 and 7.99 Debye respectively as shown in Table 2 which is expected to increase the interactivity of carboxylated and cyanide ZTRI toward adsorb atrazine.

The chemical properties of the adsorbent/adsorbate systems are highly dependent on the chosen surface plane, surface atomic termination, and molecular orientation, Adsorption energy is a decreasing of energy while two materials are combined under the adsorption process in which an atom, ion, or molecule (adsorbate) is attached to the surface of a solid (adsorbent). so, in our work, different functionalization to estimate the adsorption process, The adsorption energy was calculated as:

$$E_{\text{ads}} = ((E_G + E_{\text{Atz}}) - E_{\text{Sys}})/\text{Natoms})$$

where, E_G is the total energy of isolated ZTRI C46H18-COOH, E_{Atz} is the total energy of isolated Optimized Atrazine, E_{Sys} is the total energy of isolated Optimized Resultant, N Number of complex atoms.

Table 2 and Fig. 5 show the predicted positive adsorption energy (Ea). The calculated values validate the stability of the adsorption process of Atrazine on ZTRI and its derivatives. Chemically functionalized ZTRI was observed to have an increase in adsorption energy considerably. The adsorption energies of non-functionalized ZTRI toward Atrazine were 1.31 eV and increased to 1.28 and 1.3 eV in functionalized ZTRI by the carboxylic group and cyanide group, respectively. The calculation of adsorption energy allows us to confirm the adsorption process and compare the adsorption strength of each functionalized group.

Table 2 Calculated TDM, energy gap, and charge

Compound	Dipole moment (Debye)	Adsorption E (eV)	Adsorption E /atom (eV)	Band gap (eV)	Q charge
ZTRI C46 pristine	0.9	–	–	0.31	–
Atrazine	5.7	–	–	5.71	–
ZTRI C46-ATR	7.1	120.4	1.31	0.30	−0.02
ZTRI C46-COOH	2.8	–	–	0.29	–
ZTRI C46-COOH atrazine	3.3	121.5	1.28	0.30	0.00
ZTRI C46-CN	8.0	–	–	0.30	–
ZTRI C46-CN atrazine	16.8	121.0	1.30	0.31	−0.04

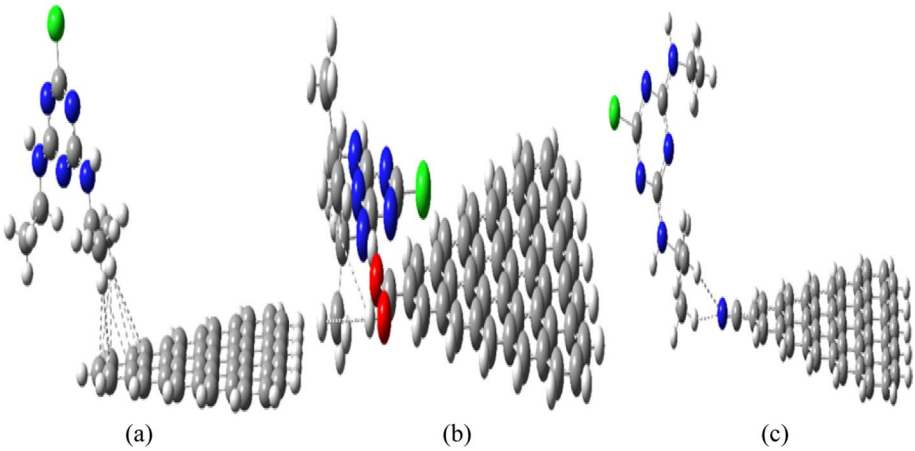

Fig. 5 Calculated adsorption of Atrazine on **a** pristine graphene edge **b** carboxylate graphene and **c** cyanide graphene

3.3 Charge transfer

The charge density differences have been calculated as the difference between the electron density of Atrazine in the complex after adsorption and before adsorption, The charge on Atrazine was after adsorption and calculated from (Q = Q total- Qin), where Q total is a charge of Atrazine and Qin is a charge of Atrazine before adsorption.

A negative Q (−0.04) value in Atrazine adsorbed in ZTRI-CN verifies that partially electron charge from ZTRI functionalized by cyanide group to Atrazine which acts as electron acceptor and graphene flakes act as electron donner.

In ZTRI functionalized by the cyanide group the nitrogen atom has five valence electrons, three of which are unpaired, and the other two form a lone pair. Usually, nitrogen forms three covalent bonds, by employing its unpaired electrons. Sometimes, by employing its lone pair, it can form a fourth covalent bond, which is dative (or coordinate), inasmuch the source of the bonding pair of electrons is only one of the two participants in the bond. In these cases, sometimes a positive charge is drawn on nitrogen (and a negative one on the other participant in the coordinate bond), as if nitrogen had nominally given an electron of its lone pair to the other atom, so that nominally now nitrogen has four unpaired electrons. On the contrary, in the case of atrazine adsorbed on ZTRI functionalized by the carboxylic group, it has a positive value of 0.004 which may come back to the hydroxyl group in the carboxylic group; oxygen is more electronegative than Hydrogen atom develops a partial positive charge (δ+) and the oxygen atom develops a partial negative charge (δ−) causing the atrazine molecule positive charge when adsorbing with ZTRI-COOH at this side.

3.4 HOMO–LUMO and energy gap analysis

HOMO and LUMO are the most essential parameters in quantum chemistry (Abdelsalam et al. 2018). In chemistry, HOMO and LUMO are types of molecular orbitals. The acronyms stand for highest occupied molecular orbital and lowest unoccupied molecular orbital, respectively, and the difference between them is called the HOMO–LUMO gap. The calculation of HOMO and LUMO gives information on the transfer of charge within

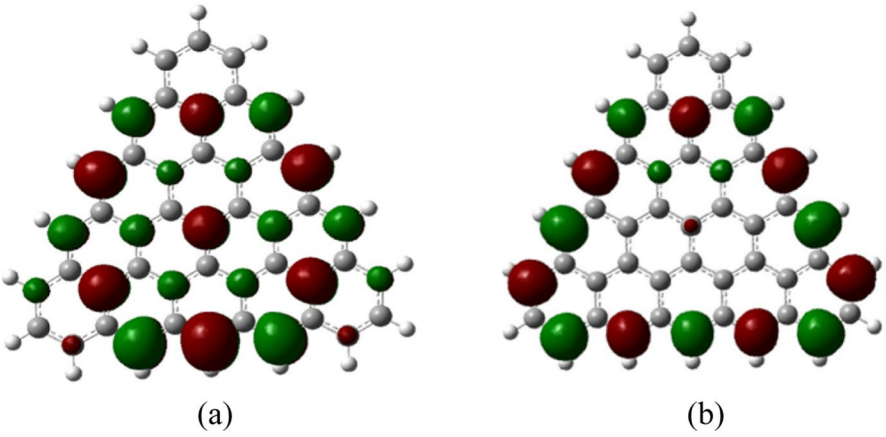

Fig. 6 **a** HOMO and **b** LUMO orbitals of ZTRI C46 pristine graphene

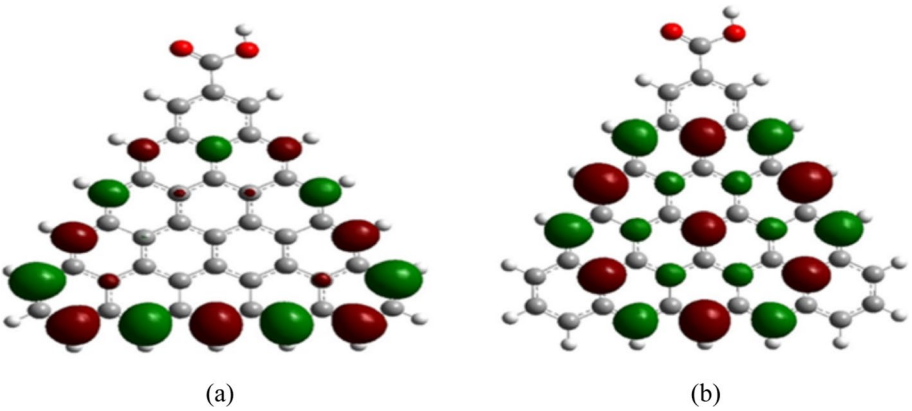

Fig. 7 **a** HOMO and **b** LUMO orbitals of ZTRI C46 functionalized with carboxyl group

the molecule (Foresman and Frisch 1996). Figure 6 presents the distribution of HOMO and LUMO. In of HOMO and LUMO, the red color denotes the positive phase while green color denotes the negative phase from the analysis, it is clear that HOMO in ZTRI is located over the center but LUMO has edge effect But in ZTRI the HOMO is localized at the zigzag edges, and the LUMO distributes over the surface of the cluster, with a relatively small band gap energy of ~ 0.31 eV, the low energy gap is due to ZTRI containing 18 hydrogen atoms the band gap decreasing first with increasing hydrogen atoms (Hiroto et al. 2014). This is caused by the splitting of energy levels of HOMO and LUMO This splitting is caused by broken symmetry in the hydrogenation to the surface (Hiroaki et al. 2011). Adding the COOH group and C≡N to ZTRI slightly decreases the band gap from 0.31 eV in pristine Graphene to 0.29 and 0.3 eV in carboxyl and cyanide functionalized ZTRI respectively and this agreed with (Abdelsalam et al. 2018; Li et al. 2018). Figures 7 and 8a, b show HOMO and LUMO of functionalized ZTRI with carboxyl and cyanide groups it seems that redistribution of orbitals without change in band gap energy values as shown in Table 2 from pristine ZTRI. There are no significant changes in band gap energy overall

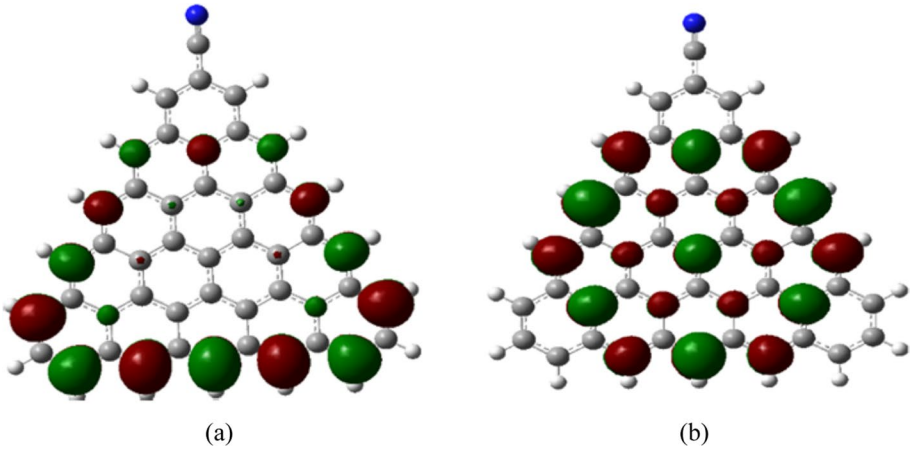

Fig. 8 **a** HOMO and **b** LUMO of ZTRI C46 functionalized with cyanide group

ZTRI, ZTRI functionalized nor adsorbed system and this is because of physical adsorption and no chemical reaction has been done to change orbital arrangements (Figs. 9, 10, 11).

3.5 Molecular electrostatic potential

Electron density is central to density functional theory (DFT). The first Hohenberg–Kohn theorem states that the electron density distribution of a system in its ground state contains all its information (Zotti et al. 2008).

The MESP contour is a physical description of the surface of each investigated structure. This might be accomplished by mapping the locations of electrophilic and nucleophilic assaults. This mapping is shown by a contour that uses colors to describe the charge distributions for the examined structure. Mapping the colors defines the site since each hue represents a different charge, thus, as the charge changes from negative to positive, the colors shift from red to blue. The color scheme red > orange represents the electronegativity > yellow > green > blue, with red indicating the highest electronegativity (highest electron density) and blue representing the lowest electronegativity (lowest electron density).

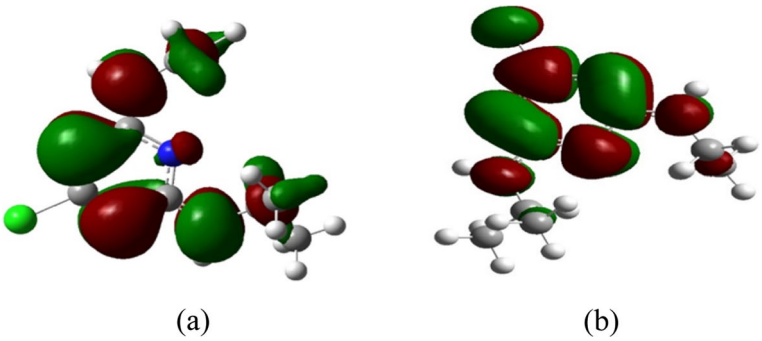

Fig. 9 **a** HOMO and **b** LUMO of optimized atrazine compound

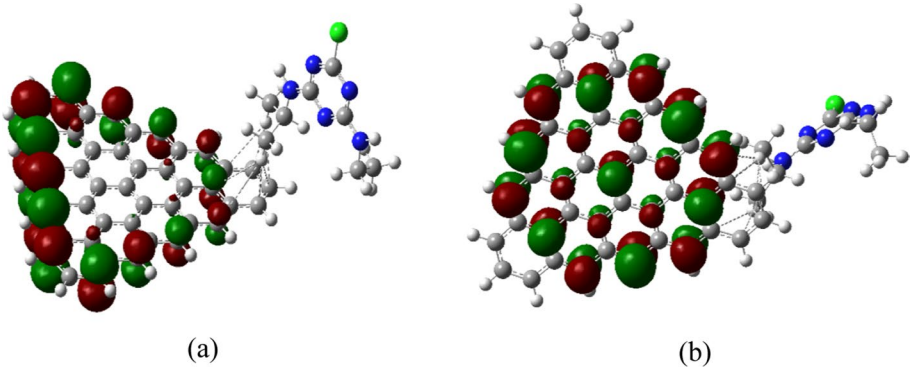

Fig. 10 **a** HOMO and **b** LUMO of optimized atrazine ZTRI after adsorption process

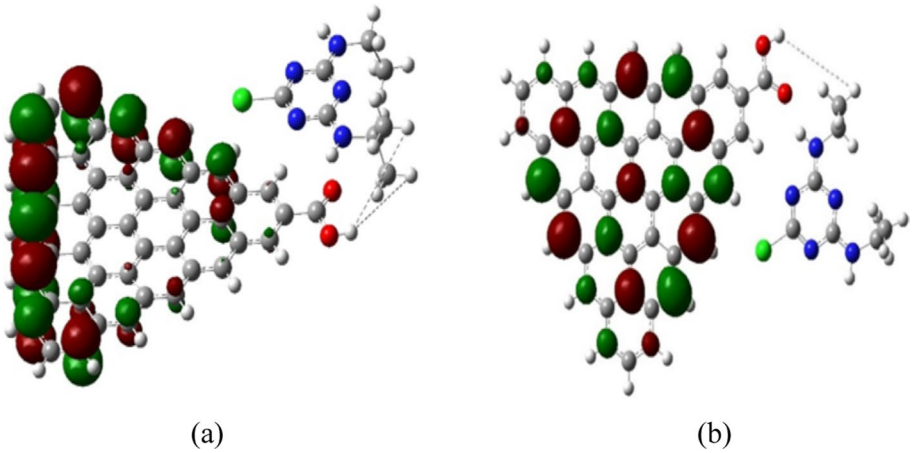

Fig. 11 **a** HOMO and **b** LUMO of optimized atrazine ZTRI functionalized with carboxylic group after the adsorption process

MESP is a useful concept in molecular modelling calculations because it can provide very accurate information on the active sites of various chemical entities (Bayoumy et al. 2020). Therefore, the MESP describes the reactivity of reactants by defining the active sites on its surface and its interaction with other molecules) Bulat et al. 2010).

The MESP map of ZTRI in Fig. 12a and b, shows the main colors in the map: red, blue, and dark blue. Red is in the centers of ZTRI in benzene-like rings in which all the ring atoms are sp^2-hybridized allowing the π electrons to be delocalized in molecular orbitals that extend around the ring, above and below the plane of the ring, forming the effect of electron delocalization phenomenon within the rings making graphene core is most probable to undergo nucleophilic interactions. Less electronegative H atoms are present in the terminals, which is why light and dark blue colors distinguish them. As a result, electrophilic reactions might take place there more frequently. While ZTRI is functionalized by a carboxyl group as shown in Fig. 12c and d, the map is characterized by two primary intense dark color active sites due to the presence of carboxyl groups. At carbonyl, part C=O is colored dark red which can be a good electrophilic active site and suitable for

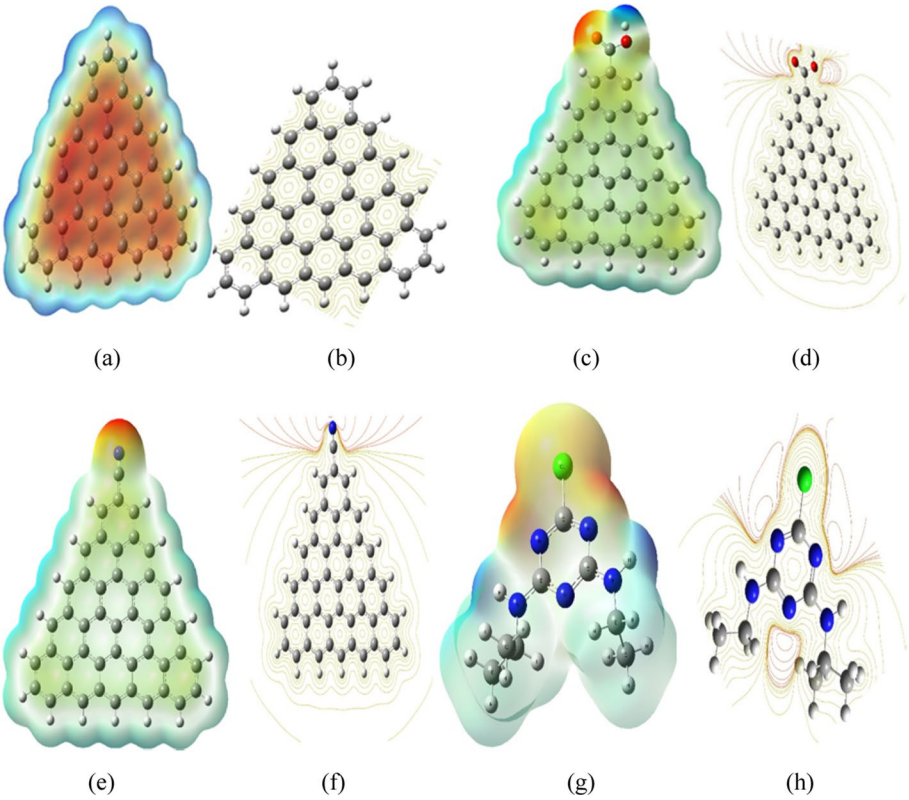

Fig. 12 MESP of **a** and **b** pristine ZTRI, **c** and **d** ZTRI functionalized by carboxyl group, **e** and **f** ZTRI functionalized by cyanide group, and **g** and **h** atrazine compound

nucleophilic attack. since oxygen is more electronegative than carbon and pulls the electron density towards itself. As a result, the carbon atom develops a partial positive charge (δ+) and the oxygen atom develops a partial negative charge (δ−), leaving the central part of Graphene almost neutral, and this charge active site concentration was the aim from functionalization of ZTRI. On the other side, the terminal H atom of the hydroxyl group region is colored dark blue color, which can be an excellent nucleophilic active site and suitable for electrophilic attack due to the exact reason for oxygen atom electronegativity.

ZTRI functionalized by a cyanide group Map characterized by only one red active site on the nitrogen atom as shown in Fig. 12e and f. The atrazine MESP maps in Fig. 12g and h show that the nitrogen atom within the benzene ring is red but terminal H atoms linked with nitrogen outside the benzene ring show blue color.

3.6 Infrared spectra

The B3LYB/3-21G computed IR spectra for ZTRI, modified with carboxyl groups and cyanide to the edges, are shown in Fig. 13a–c. The vibrational spectra are calculated in order to verify that the electronic properties previously computed are calculated on

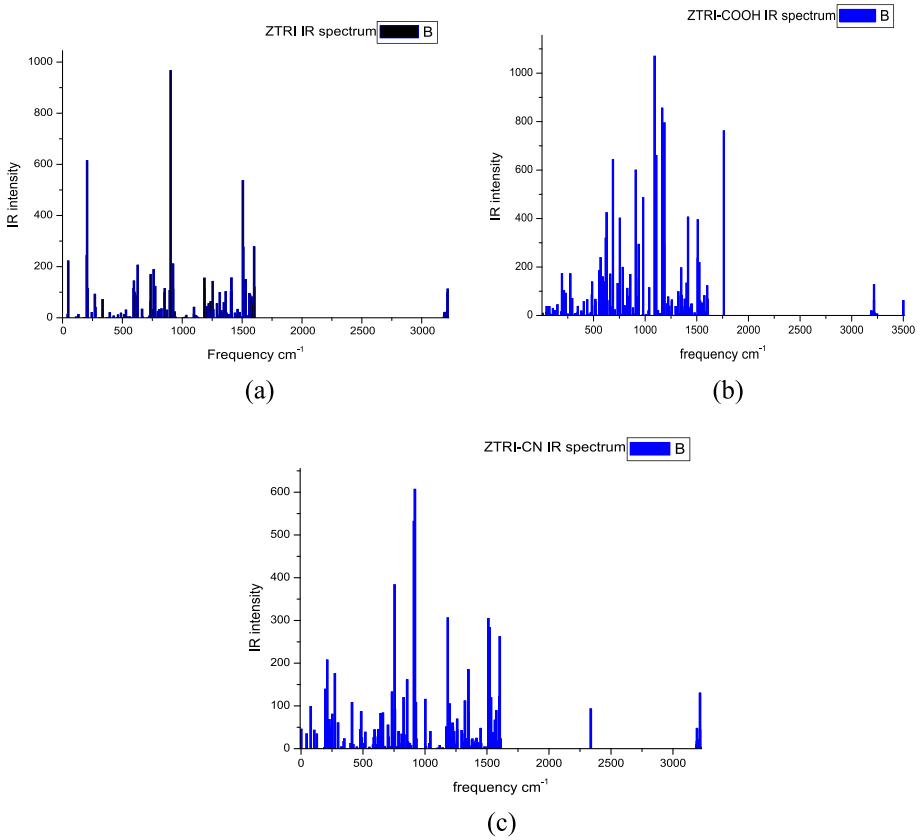

Fig. 13 B3LYP/3-21G computed IR spectra of **a** ZTRI, **b** ZTRI activated by COOH group, and **c** ZTRI activated by cyanide group

optimum structures. Figures 13, 14, and 15 show no negative frequencies, hence the information from the earlier sections is supported by the recorded positive frequencies.

3.7 Calculated DFT energy

Although IR calculations are a good test for the optimization of the studied structures which confirm that the structures are optimal structures. Thermochemical energy will be introduced also. As a descriptor for the thermochemistry, the energy is reported in DFT calculations the method is denotes the method used to obtain this energy. In this sense the obtained energy is termed as E(RB3LYP) as indicated in Table 3. Beside energy the table presented also the RMS gradient norm.

Resulted data in Table 3 indicated that, the studied structure even after interaction with Atrazine are thermally stable.

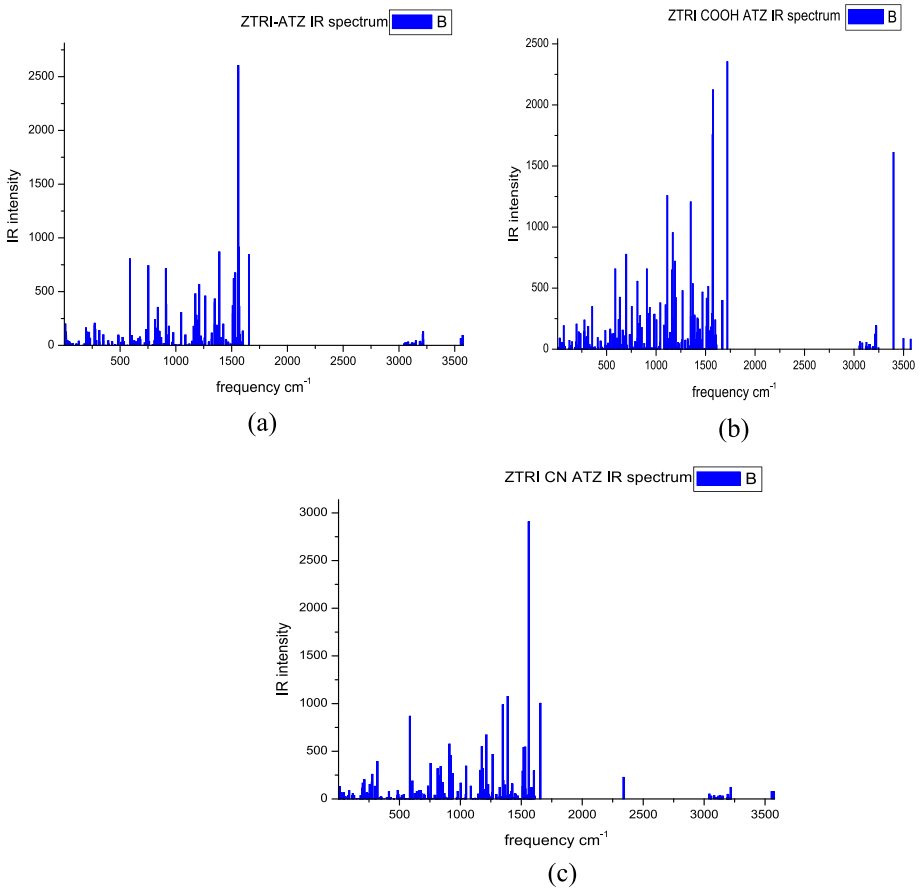

Fig. 14 B3LYP/3-21G computed IR spectra of adsorbed atrazine on **a** ZTRI, **b** ZTRI activated by COOH group, and **c** ZTRI activated by cyanide

4 Conclusion

The graphene triangle shape ZTRI was studied its capability to adsorb Atrazine from water. The chemical reactivity of ZTRI was improved by adding activated groups like carboxyl and cyanide groups. Carboxyl and cyanide groups were added to increase the selectivity, sensitivity, and adsorption capacity of ZTRI toward atrazine pollutants. This modification allows the electrochemical reaction to occur at a lower potential range. The electrical properties of the proposed models and their interactions were studied in terms of TDM, ΔE, and MESP, and results indicated that the electrical properties have improved since TDM has increased, ΔE has slightly decreased, and electronegativity has significantly improved. At the interaction of ZTRI with Carboxyl and cyanide groups, the TDM increased from 0.9 Debye in pristine ZTRI to 2.8 and 8 Debye, respectively, and ΔE decreased from 0.31 to 0.3 eV by 0.01 eV, with high electronegativity demonstrated in MESP maps. Successful adsorption of Atrazine on functionalized ZTRI by obtained positive adsorption energy ranging from 1.28 to 1.31 eV. The positive frequencies from drawing the IR spectra indicated that all calculations were done in optimum structures.

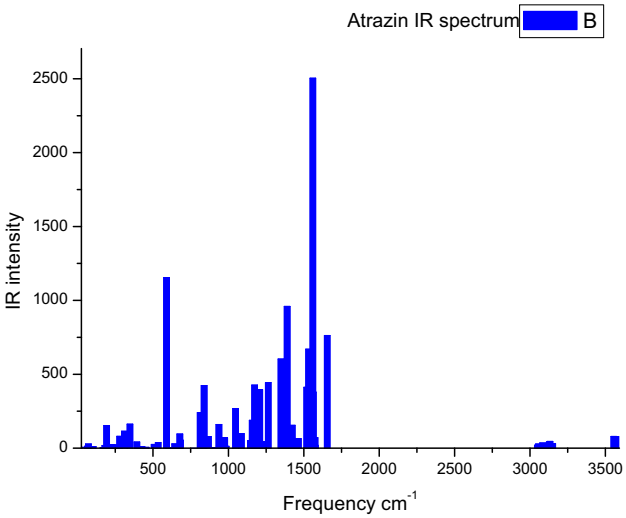

Fig. 15 B3LYP/3-21G computed IR spectrum of Atrazine

Table 3 B3LYP/3-21G calculated energy E(RB3LYP) and RMS gradient norm

Compound	E (Hartree)	RMS gradient norm (Hartree/Bohr)
ZTRI C46 pristine	− 1754.1	0.000162
Atrazine	− 1037.4	0.000013
ZTRI C46-ATR	− 2795.9	0.000006
ZTRI C46-COOH	− 1941.6	0.000029
ZTRI C46-COOH atrazine	− 2983.5	0.000004
ZTRI C46-CN	− 1845.8	0.000102
ZTRI C46-CN atrazine	− 2887.6	0.000004

Correlating the calculated energy with IR data, one can conclude that the studied structures are optimized and thermally stable.

Acknowledgements The authors would like to thank the Molecular Modeling and Spectroscopy Laboratory at the Centre of Excellence for Advanced Science, National Research Centre, Egypt, for the computational facilities provided in this work.

Authors' contributions The authors contribute equally to the manuscript.

Funding Open access funding provided by The Science, Technology & Innovation Funding Authority (STDF) in cooperation with The Egyptian Knowledge Bank (EKB). This research received no external funding.

Availability of data and materials The data will be available upon request; contact Medhat A. Ibrahim medahmed6@yahoo.com.

Declarations

Conflict of interest The authors declare no conflict of interest.

Ethical approval This work does not apply to both human and/or animal studies.

References

Abdelsalam, H., Elhaes, H., Ibrahim, M.: First-principles study of edge carboxylated graphene quantum dots. Physica B **537**, 77–86 (2018). https://doi.org/10.1016/j.physb.2018.02.001

Abhilash, P.C., Singh, N.: Pesticide use and application: an Indian scenario. J. Hazard. Mater. (2009). https://doi.org/10.1016/j.jhazmat.2008.10.061

Allran, J.W., Karasov, W.H.: Effects of atrazine and nitrate on northern leopard frog (Rana pipiens) larvae exposed in the laboratory from posthatch through metamorphosis. Environ. Toxicol. Chem. (2009). https://doi.org/10.1002/etc.5620191133

Axel, D.B.: Density-functional thermochemistry. III. The role of exact exchange. J. Chem. Phys. **98**(7), 5648–5652 (1993). https://doi.org/10.1063/1.464913

Bayoumy, A.M., Ibrahim, M., Omar, A.: Mapping molecular electrostatic potential (MESP) for fulleropyrrolidine and its derivatives. Opt. Quant. Electron. **346**, 52 (2020). https://doi.org/10.1007/s11082-020-02467-6

Bulat, F.A., Toro-Labbé, A., Brinck, T., Murray, J.S., Politzer, P.: Quantitative analysis of molecular surfaces: areas, volumes, electrostatic potentials and average local ionization energies. J. Mole. Model. **11**, 1679–1691 (2010). https://doi.org/10.1007/s00894-010-0692-x

Burnside, O., Wicks, G.: Atrazine carryover in soil in a reduced tillage crop production system. Weed Sci. **28**(6), 661–666 (1980). https://doi.org/10.1017/S0043174500061464

Carsel, F.R., Nixon, B.W., Ballantyne, L.G.: Comparison of pesticide root zone model predictions with observed concentrations for the tobacco pesticide metalaxyl in unsaturated zone soils. Environ. Toxicol. Chem. (1985). https://doi.org/10.1002/etc.5620050403

Christian, E.W., Renate, L., Spieser, H.: Effects of atrazine on the swimming behavior of zebrafish, Brachydanio rerio. Water Res. **3**(29), 981–985 (1995). https://doi.org/10.1016/0043-1354(94)00217-U

Compton, O.C., Nguyen, S.T.: Graphene oxide, highly reduced graphene oxide, and graphene: versatile building blocks for carbon-based materials. Small **6**(6), 711–723 (2010). https://doi.org/10.1002/smll.200901934

Das, S., Sakr, H., Al-Huseini, I., Jetti, R., Al-Qasmi, S., Sugavasi, R., Sirasanagandla, S.R.: Atrazine toxicity: the possible role of natural products for effective treatment. Plants **12**(12), 2278 (2023). https://doi.org/10.3390/plants12122278

Fan, H., Zhou, S., Wei, Q., Hu, X.: Honeycomb-like carbon for electrochemical energy storage and conversion. Renew. Sustain. Energy Rev. (2022). https://doi.org/10.1016/j.rser.2022.112585

Foresman, J.B., Frisch, A.E.: Exploring Chemistry with Electronic Structure Methods, 2nd edn. Gaussian, Pittsburgh (1996)

Frisch, J., Trucks, H.B., Scuseria, G.E., Robb, M.A., Cheeseman, J., Scalmani, G., Barone, V., Mennucci, B., Petersson, G.A., Nakatsuji, H., Caricato, M., Li, X., Hratchian, H.P., Izmaylov, J.: Gaussian 09 Revision A.1. Gaussian Inc. (2009).

Geim, A., Novoselov, K.: Effects of atrazine on the swimming behavior of zebrafish. Nat. Mater. **6**, 183–191 (2007). https://doi.org/10.1038/nmat1849

Hasnip, P.J., Refson, K., Probert, M.I., Yates, J.R., Clark, S.J., Pickard, C.J.: Density functional theory in the solid state. Philos. Trans. r. Soc. **372**(2011), 20130270 (2014). https://doi.org/10.1098/rsta.2013.0270

Hiroaki, N., Atsushi, M., Seiki, S., Arimichi, T., Yuichi, T., Noriyasu, O., Shin, K.: Molecular dynamics simulation of hydrogen injection onto diamond surfaces. J. Appl. Phys. **50**, 151 (2011). https://doi.org/10.1143/JJAP.50.01AB04

Hiroto, T., Tetsuji, L., Hiroshi, K.: Effect of hydrogenation on the band gap of graphene nano-flakes. Thin Solid Films **554**, 199–203 (2014). https://doi.org/10.1016/j.tsf.2013.08.108

Hohenberg, P., Kohn, W.: Inhomogeneous electron gas. Am. Phys. Soc. Phys. Rev. **136**, 864 (1964). https://doi.org/10.1103/PhysRev.136.B864

Huizar, M., Luis, H., Rios, R., Clara, H., Olvera-Maturano, N.J., Juvencio, R., Rodriguez, J.A.: Chemical reactivity of quinclorac employing the HSAB local principle—Fukui function. Open Chem. (2015). https://doi.org/10.1515/chem-2015-0008

Karr, J.R., Chu, E.W.: Sustaining living rivers. Hydrobiologia **1**(14), 422 (2000). https://doi.org/10.1023/A:1017097611303

Kohn, W., Sham, L.: Self-consistent equations including exchange and correlation effects. Phys. Rev. Rev **140**, A1133–A1138 (1965). https://doi.org/10.1103/PhysRev.140.A1133

Li, H., Zhang, Z., Liu, Y., Cen, W., Luo, X.: Functional group effects on the HOMO-LUMO Gap of g-C_3N_4. NanomateRials (basel, Switzerland) **8**(8), 589 (2018). https://doi.org/10.3390/nano8080589

Mariane, R.S., Seibert, D., Beatriz, H.Q., Bassetti, M., Fátima, F., Fagundes-Klen, R., Rosângela Bergamasco, R.: Occurrence, impacts and general aspects of pesticides in surface water: a review. Process. Saf. Environ. Prot. **125**, 22–37 (2020). https://doi.org/10.1016/j.psep.2019.12.035

McCormick, L., Hiltbold, A.E.: Microbiological decomposition of atrazine and diuron in soil. Weeds **14**(1), 77–82 (1966). https://doi.org/10.2307/4041129

Michael, E., Thurman, D.A., Goolsby, M.T., Mills, M.S., Pomes, M.L., Dana, W.J.: A reconnaissance study of herbicides and their metabolites in surface water of the midwestern United States using immunoassay and gas chromatography/mass spectrometry. Environ. Sci. Technol. **26**(12), 2440–2447 (1992). https://doi.org/10.1021/es00036a016

Ouellette, R., Rawn, D.: Organic Chemistry: Structure, Mechanism, Synthesis. Elsevier Science. 1st edn–June 6 (2014)

Rudberg, E., Sałek, P., Luo, Y.: Nonlocal exchange interaction removes half-metallicity in graphene nanoribbons. Nano Lett. **8**, 2211–2213 (2007). https://doi.org/10.1021/nl070593c

Sass, J.B., Colangelo, A.: European Union bans atrazine, while the United States negotiates continued use. Int. J. Occupat. Health **12**(3), 260–267 (2006). https://doi.org/10.1179/oeh.2006.12.3.260

Xiaolei, Q., Pedro, J., Qilin, L.: Applications of nanotechnology in water and wastewater treatment. Water Res. **47**(12), 3931–3946 (2013). https://doi.org/10.1016/j.watres.2012.09.058

Xu, P., Zeng, G.M., Huang, D.L., Feng, C.L., Hu, S., Zhao, M.H., Lai, C., Wei, Z., Huang, C., Xie, G.X., Liu, Z.F.: Use of iron oxide nanomaterials in wastewater treatment: a review. Sci. Total. Environ. **1**(424), 1–10 (2012). https://doi.org/10.1016/j.scitotenv.2012.02.023

Yang, W., Ratinac, K.R., Ringer, S.P., Thordarson, P., Gooding, J.J., Braet, F.: Carbon nanomaterials in biosensors: should you use nanotubes or graphene? Biosensors Carbon Nanomater. **49**(12), 2114–2138 (2010). https://doi.org/10.1002/anie.200903463

Zhang, Q., Uchaker, E., Candelaria, S.L., Cao, G.: Nanomaterials for energy conversion and storage. Chem. Soc. Rev. **42**(7), 3127–3171 (2013a). https://doi.org/10.1039/C3CS00009E

Zhang, Y., Nayak, T.R., Hong, H., Cai, W.: Biomedical applications of zinc oxide nanomaterials. Curr. Mol. Med. **10**, 1633–1645 (2013b). https://doi.org/10.2174/15665240130666131111130058

Zotti, L.A., Teobaldi, G., Palotás, K., Ji, W., Gao, H.J., Hofer, W.A.: Adsorption of benzene, fluorobenzene and meta-di-fluorobenzene on Cu(110): a computational study. J. Comput. Chem. **29**(10), 1589–1595 (2008). https://doi.org/10.1002/jcc.20916